Electrochimica Acta 55 (2010) 6818–6829

Contents lists available at ScienceDirect

Electrochimica Acta

journal homepage: www.elsevier.com/locate/electacta

Characterisation of a re-cast composite Nafion® 1100 series of proton exchange membranes incorporating inert inorganic oxide particles

S.M. Slade[a], J.R. Smith[a], S.A. Campbell[a], T.R. Ralph[b,c], C. Ponce de León[c], F.C. Walsh[c,*]

[a] School of Pharmacy and Biomedical Sciences, University of Portsmouth, St. Michael's Building, White Swan Road, Portsmouth PO1 2DT, United Kingdom
[b] Johnson Matthey Fuel Cells, Lydiard Fields, Great Western Way, Swindon SN5 8AT, United Kingdom
[c] Electrochemical Engineering Laboratory, Energy Technology Research Group, School of Engineering Sciences, University of Southampton, Highfield, Southampton SO17 1BJ, United Kingdom

ARTICLE INFO

Article history:
Received 16 February 2010
Received in revised form 23 May 2010
Accepted 29 May 2010
Available online 4 June 2010

Keywords:
Atomic force microscopy
Conductivity
Composites
Ion-exchange membranes
PEM fuel cell

ABSTRACT

A series of cation exchange membranes was produced by impregnating and coating both sides of a quartz web with a Nafion® solution (1100 EW, 10%wt in water). Inert filler particles (SiO_2, ZrO_2 or TiO_2; 5–20%wt) were incorporated into the aqueous Nafion® solution to produce robust, composite membranes. Ion-exchange capacity/equivalent weight, water take-up, thickness change on hydration and ionic and electrical conductivity were measured in 1 mol dm^{-3} sulfuric acid at 298 K. The TiO_2 filler significantly impacted on these properties, producing higher water take-up and increased conductivity. Such membranes may be beneficial for proton exchange membrane (PEM) fuel cell operation at low humidification. The PEM fuel cell performance of the composite membranes containing SiO_2 fillers was examined in a Ballard Mark 5E unit cell. While the use of composite membranes offers a cost reduction, the unit cell performance was reduced, in practice, due to drying of the ionomer at the cathode.

1. Introduction

Perfluorinated ion-exchange membranes, such as Nafion® materials (DuPont de Nemours), have a high ionic conductivity and are capable of operating at a high current density; these materials also show a high (electro)chemical and mechanical stability [1–3]. Such membranes are routinely employed in proton exchange membrane (PEM) fuel cells, which are used in transportation (<75 kW), stationary (5–10 kW or <250 kW) or back-up power (1–3 kW) [4]. The membranes are also used in many other areas, including gas sensing, gas separation, electrodialysis and salt-splitting [5–10].

Water management in ion-exchange membranes is critical for efficient performance, since full hydration ensures optimum proton conduction [1,11] while flooding leads to many operational problems. Such membranes show a high permselectivity to cations and their water/electrolyte uptake can vary over a wide range [12]. The materials contain both a fluorocarbon phase and an ionic phase (with associated water molecules). Upon water uptake, membranes generally undergo a phase separation into an amorphous hydrophilic phase containing the hydrated sulfonic acid groups and a crystalline, hydrophobic phase formed by the perfluorinated polymer backbone [13–15].

The ionic conductivity of extruded Nafion® membranes decreases (non-linearly) with film thickness due to the electrode–membrane contact resistance and uneven water distribution in the membranes leading to surface and bulk membrane conductivity differences [16]. Membranes re-cast from propan-2-ol and butan-1-ol, immersed in H_2SO_4 (1 mol dm^{-3}) at 298 K, showed higher conductivities than the extruded membranes. The higher conductivity may be attributed to differences in polymer structure caused by solvent drying rates and polymer–solvent interactions [17].

Nafion® membranes can also be modified by the addition of inorganic substances, often by sol–gel reactions involving the formation of Nafion® and silica hybrids from solution, followed by growth of the inorganic phase by hydrolysis/condensation of alkoxy silanes [18]. *In-situ* sol–gel reactions have also been performed, where the Nafion® membrane is swollen by solvent incorporation using, for example, methanol/water mixtures; then the polymer structure is permeated by a tetraethylorthosilicate monomer. Water initiates the *in-situ* sol–gel reaction; upon drying (heat and vacuum), volatiles are removed, driving the condensation of the ≡SiOH groups [19]. Although sol–gel reactions have been investigated, little work has been carried out on the influence of this process on the resultant ionic resistivity (ρ) of the membranes.

Zoppi and Nunes have suggested that the incorporation of a silica network into the basic Nafion® structure could improve the thermal and mechanical properties of the material and increase the amorphous content. It was proposed that the addition of silica would modify the polymer properties of Nafion® [18] and

* Corresponding author. Tel.: +44 23 8059 8752; fax: +44 23 8059 8754.
E-mail address: F.C.Walsh@soton.ac.uk (F.C. Walsh).

0013-4686/$ – see front matter © 2010 Elsevier Ltd. All rights reserved.
doi:10.1016/j.electacta.2010.05.085

improve the ionic conductivity. This enhancement is considered to involve increased mobility of the charge carriers within the membrane. Mauritz studied the effect of *in-situ* sol–gel reactions between the alkoxides of silicon, titanium, aluminium, zirconium and organoalkoxysilanes with Nafion® as a means of enhancing mechanical and wear properties as well as increasing the thermal and environmental stability of the membranes [19]. Tiwari et al. studied Nafion® 117 containing inorganic ion-exchangers, including zirconium phosphate and zirconium oxide (ZrO_2), to increase the ion-exchange capacity and thermal stability of Nafion® [20]. ZrO_2 was chosen due to its behaviour as an anion-exchanger in acidic and neutral medium and as a cation exchanger in alkaline solutions [20].

Ion-exchange membranes incorporating zirconium phosphate have been shown to significantly enhance performance at elevated temperatures due to the hygroscopic nature of the salt in retaining water within the membrane structure [21,22]. Watanabe et al. developed a modified Nafion® membrane containing a nanocrystallite dispersion of silicon dioxide (SiO_2), titanium dioxide (TiO_2) and platinum particles [23]. This helped to obviate water management problems encountered with PEMFCs and to reduce the gaseous hydrogen and oxygen crossover through the thinner membranes adopted for improved performance. Platinum provided active sites to catalytically combine H_2 and O_2 and the resulting water product was retained by the hygroscopic oxides, enabling the PEM fuel cell to be operated (under limited conditions) without external humidification.

Studies have also been carried out on perfluorinated ionomer composite membranes, such as those reinforced with woven poly(tetrafluoroethylene) (PTFE). These composites are mainly used in industrial electrolysis. The relatively coarse weave of the woven PTFE support results in membranes which are too thick to show a reasonable potential drop for fuel cell applications. Composite membranes which have been formulated for use in fuel cells include the Gore-Select® series, which have a non-woven PTFE/fluorocarbon composition [24]. In a separate approach, it has been shown that a reduction in the Nafion® content and the presence of an inorganic filler can improve membrane performance [25]. The incorporation of inorganic fillers into an ion-exchange membrane can also result in significant cost savings (due to the lower cost of the fillers compared to Nafion polymer) and a more robust, composite ion-exchange material.

This paper considers a range of composite membranes containing a quartz web impregnated, coated and sprayed with solutions of Nafion® ionomer (1100 EW series; 10%wt in water), in the absence and presence of an inert filler (SiO_2, ZrO_2 or TiO_2; 5–10%wt). A wide range of physico-chemical and electrochemical techniques are used to characterise the composite membranes. The ion-exchange capacity (IX)/equivalent weight (EW) were measured and the hydration number (λ), thickness change and proton conductivity investigated in 1 mol dm^{-3} H_2SO_4 at 298 K. The membrane structure was examined using scanning electron microscopy (SEM) and atomic force microscopy (AFM). Two sheets of composite membrane were laminated together to improve the gas tightness of the membrane for PEM fuel cell operation. The PEM unit cell performance of the SiO_2-filled membranes was examined in a Ballard Mark 5E unit cell using membrane electrode assemblies (MEAs) manufactured in-house.

2. Experimental

2.1. Chemicals and reagents

Hydrogen peroxide (2%wt), sulfuric acid, phosphorus pentoxide, potassium chloride, nickel chloride, copper chloride and cobalt chloride (all Analar grade) were obtained from Fisher (Loughborough, UK). Sodium chloride (Analar), sodium hydroxide (Analar) and phenol red were obtained from Sigma–Aldrich (Poole, Dorset, UK). A Sanyo Fistream Cyclon unit provided doubly distilled water with conductivity greater than 20 MΩ cm.

2.2. Membrane manufacture

Sheets of membrane (550 cm^2, 22 cm × 25 cm) were manufactured at a target thickness of 30 μm using a silica casting tray. A web of quartz fibres with a density of 0.65 mg cm^{-2} was prepared using paper making technology. The quartz fibres (0.42 g) were dispersed in demineralised water (400 cm^3) and the mixture poured into the damn of the laboratory paper maker fitted with a supporting mesh at the bottom of the damn. After removal of the water the quartz web and mesh were released from the damn and sprayed with a Nafion® solution (1100 EW, 5%wt in alcohol/water), supplied by DuPont de Nemours (Delaware, USA) to bind the fibres together. The sheet was dried at 105 °C in an oven to produce a dry Nafion® loading of typically 20–30%wt. The sheet was then immersed in an aqueous Nafion® solution (1100 EW, 10%wt in water) manufactured in-house, in the casting tray, to impregnate and to coat both faces of the quartz sheet. After drying in a vacuum oven at 60 °C for 3 h and final air drying at room temperature both faces of the sheet were sprayed with the aqueous Nafion® solution to ensure complete coverage of the quartz fibres. After drying in air at room temperature sheets of membrane were heated in air at 150 °C to anneal the polymer. Two annealed membrane sheets were laminated together at 175 °C to form a composite membrane for PEM fuel cell testing.

Composite membranes were manufactured from aqueous Nafion® (1100 EW, 5 and 10%wt) containing filler metal oxides. Again, the composite membranes employed the organic Nafion® bound quartz web and were prepared by impregnation, spraying, annealing and final lamination of two sheets together, as outlined above. The metal oxides investigated included: three types of SiO_2: 'SiO_2-A' (Ludox® from Grace Davison, St. Neots, Cambridgeshire, UK, with BET 230 m^2 g^{-1}), 'SiO_2-B' (Syton® from Grace Davison, St. Neots, Cambridgeshire, UK with BET 265 m^2 g^{-1}) and 'SiO_2-C' (Aerosil® from Evonik Industries AG, Essen, Germany, with BET 300 m^2 g^{-1}), 'ZrO_2' from Sigma–Aldrich, Poole, Dorset, UK with BET 25 m^2 g^{-1} and two types of TiO_2 ('TiO_2-A' and 'TiO_2-B' obtained as titanium iso-propoxide from Sigma–Aldrich, Poole, Dorset, UK with an average BET of 15 m^2 g^{-1}). The specific surface area, BET was determined by nitrogen gas adsorption.

'SiO_2-A' and 'SiO_2-B' dispersions were diluted with water to give 5%wt, 10%wt and 20%wt solutions. Sodium-stabilised silicas were avoided since these precipitated on standing. The dispersions were added directly to aqueous Nafion® (1100 EW, 10%wt) to form gels, which were re-dissolved in water to produce the ionomer solutions for membrane casting. Membrane sheets were cast, spray coated and annealed as detailed above for the composite membrane containing no metal oxide additive to give a silica loading of 5%wt, 10%wt and 20%wt with respect to the dry Nafion® ionomer weight. 'SiO_2-C' and 'ZrO_2' solids were each dissolved in water at 5%wt (the 10%wt level caused some precipitation) and the resultant dispersions used, as detailed above for the 'SiO_2-A' and 'SiO_2-B' dispersions, to give membrane sheets containing 5%wt silica or 5%wt zirconia, with respect to the dry Nafion® ionomer weight.

'TiO_2-A' was prepared by adding titanium iso-propoxide dropwise to iso-propyl alcohol (IPA) to give a 1–2%wt colloidal dispersion which was distilled with organic Nafion® solution (1100 EW, 5%wt in IPA/water) under a N_2 blanket to remove all of the alcohols. The alcohol dissolved the quartz web during subsequent membrane casting. After distillation, the 'TiO_2-A' containing aqueous Nafion® solution was evaporated to give a 5%wt or 10%wt

Table 1
Composition of composite membranes.

Membrane sample number	Filler material	[Nafion® resin] (%wt)	[SiO_2] (%wt)	[ZrO_2] (%wt)	[TiO_2] (%wt)	Dry membrane thickness (μm)
1	None (unfilled cast Nafion® membrane)	91.0	0	0	0	34
2	SiO_2-A (5%wt)	86.6	4.6	0	0	28
3	SiO_2-A (10%wt)	82.6	9.2	0	0	29
4	SiO_2-A (20%wt)	70.6	20.4	0	0	31
5	SiO_2-B (5%wt)	86.3	4.6	0	0	34
6	SiO_2-B (10%wt)	82.0	9.0	0	0	33
7	SiO_2-C (5%wt)	86.7	4.6	0	0	34
8	SiO_2-C (10%wt)	81.7	4.5	0	0	33
9	ZrO_2-A (5%wt)	87.0	0	4.6	0	30
10	TiO_2-A (5%wt)	86.0	0	0	4.5	34
11	TiO_2-A (10%wt)	82.0	0	0	9.0	33
12	TiO_2-B (5%wt)	86.6	0	0	4.6	34
13	TiO_2-B (10%wt)	82.0	0	0	9.0	32

'TiO_2-A' loading based on the dry Nafion® ionomer weight in the membrane sheet. While there was no significant evidence of precipitation initially, on standing overnight there were signs of poor stability. This was attributed to the breakdown of 'TiO_2-A'–Nafion® interactions during the distillation. Consequently, 'TiO_2-B' was prepared by adding the 1–2%wt colloidal dispersion of titanium iso-propoxide in IPA to aqueous Nafion® (1100 EW, 5%wt) with stirring and allowing the mixture to slowly evaporate at room temperature to remove the IPA and to slowly hydrolyse the titanium iso-propoxide to titanium hydroxide. The concentration of the'TiO_2-B' in the solution was adjusted to 5%wt or 10%wt relative to the dry Nafion® weight to give the ionomer solution for membrane sheet production. Table 1 summarises the composition of the cast membrane sheets manufactured in this study.

2.3. Membrane pre-treatment

All membranes were pre-treated by immersing them in 2%wt H_2O_2 for 2 h at 353 K followed by cooling and rinsing in water then soaking in H_2SO_4 (0.5 mol dm^{-3}) for 48 h. The materials were rinsed in water, treated at 353 K in aqueous H_2SO_4 (0.02 mol dm^{-3}) for 1 h, rinsed with water, then stored in water at 298 K until required.

2.4. Ion-exchange capacities and equivalent weights

Pre-treated membrane samples of known weight (*ca.* 1 g) were placed in aqueous NaCl (50 cm^3, 0.1 mol dm^{-3}) for 24 h to allow conversion of the ionomer from the H^+ to the Na^+ form. The membrane samples were removed and dried (P_2O_5) in a closed container at 295 K for 48 h then re-weighed. The resulting HCl solution was titrated against NaOH (0.02 mol dm^{-3}) to an end-point of pH 7 using phenol red indicator. The volume of NaOH consumed was used to calculate the amount of H^+ in solution and, assuming complete cation exchange, the IX (the number of fixed ionic groups per unit mass of the membrane) and EW (mass of polymer containing a unit amount of fixed SO_3H groups) was calculated from the relationships [26]:

$$\mathrm{IX} = \frac{V_{\mathrm{NaOH}} \times m_{\mathrm{NaOH}}}{w} \quad (1)$$

where V_{NaOH} and m_{NaOH} are the volume and concentration of the NaOH solution while w is the mass of dried polymer membrane.

$$\mathrm{EW} = \frac{1}{\mathrm{IX}} \quad (2)$$

2.5. Water content

Samples of wet pre-treated membrane, soaked for 24 h in the solution of interest, were taken and carefully blotted dry of all surface moisture then weighed to ±0.0001 g. The membrane samples were suspended over P_2O_5 at 295 ± 2 K in a closed container for 48 h then re-weighed. The membrane water content, λ (mol H_2O/SO_3H group), was calculated *via*:

$$\lambda = \frac{\mathrm{EW}(w_1 - w)}{M_{\mathrm{R}}(\mathrm{H_2O})w} \quad (3)$$

where w_1 is the mass of the hydrated membrane, w is the mass of dried polymer and M_{R} (H_2O) is the relative molar mass of water.

2.6. Thickness measurements

Membrane thickness in the atmospherically dry state was measured using a digital micrometer (Mitutoyo, digimatic micrometer) at 295 K and ambient humidity. Membranes dried over P_2O_5 were considered to be fully dry; due to the hygroscopic nature of the polymers, the membranes re-hydrated almost immediately on contact with humid air. Hydrated membrane thicknesses (10 measurements on 5 areas) were measured after membranes were soaked overnight in the test electrolyte at 295 ± 2 K.

2.7. DC ionic resistance

A glass electrochemical cell (Fig. 1) connected to a galvanostat (Autostat, Sycopel, Newcastle upon Tyne, UK) and a waveform generator (PPR1, Hi-Tek, Southampton, UK) were used to measure the *j*–*E* characteristics (linear sweep: 0–1000 mA cm^{-2}, 5 mA s^{-1}) of the membrane at ambient temperature (295 ± 2 K). Samples (*ca.* 2 cm × 2 cm) were placed between the silicone rubber gaskets and the cell components were clamped together. Two Pt gauze counter electrodes each having a projected area approximately equal to 4 cm^2 were positioned on either side of the membrane and two matched, saturated calomel electrodes (SCE) were used as reference electrodes. The electrolyte was H_2SO_4 (60 cm^3, 1.0 mol dm^{-3}). The potential difference across the membrane as a function of current was recorded (five measurements per membrane). A linear plot was obtained, allowing the averaged resistance to be measured from the slope. In order to allow for the contribution of the electrolyte, uncompensated resistance measurements were subtracted from the measured value to establish the true ionic resistivity (ρ) of the membrane.

2.8. Solid-state resistivity

All the membranes were kept at 298 ± 2 K and ambient humidity for a minimum of 12 h before measurements were performed. Solid-state membrane resistivities (5 cm × 5 cm, 15 measurements per sample) were obtained using an in-line four-point probe (Jandel Universal four-point probe) using a 30 g loading force. A small

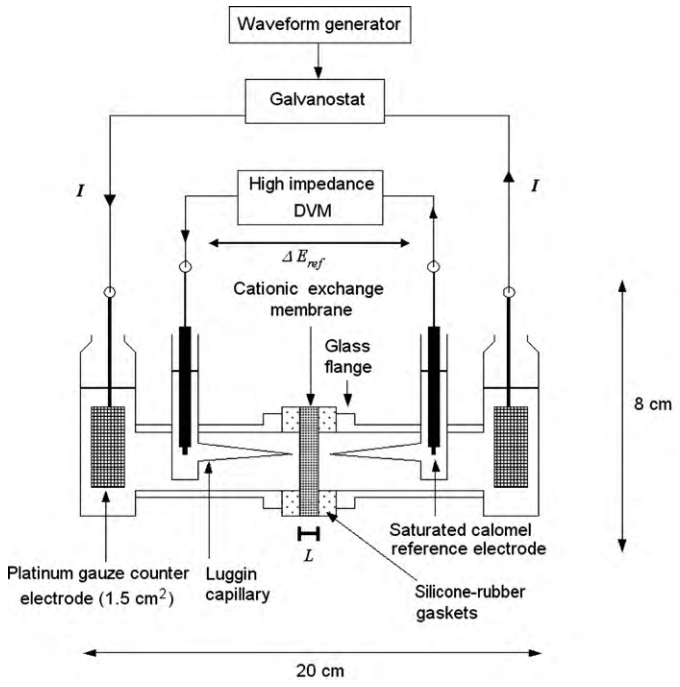

Fig. 1. The four-electrode glass cell used for conductivity measurements on a circular section (1 cm^2) of membrane, using a steady state linear sweep galvanodynamic technique. After [17].

AC current (10 mA, HP4263A LCR meter) was passed between the two outer pins (spacing 0.1 cm) and the potential difference was measured across the two inner pins.

2.9. Scanning electron microscopy

Samples of surface dry membrane were mounted on double-sided (electrically conductive) carbon tape located on brass SEM stubs. The samples were placed in a vacuum oven for 24 h at 298 ± 2 K. Samples were coated with gold/palladium and imaged using a scanning microscope microscopy (SEM; Jeol JSM 6100, MA, USA).

2.10. Atomic force microscopy

Membrane samples (1 cm × 1 cm sections) were fixed on a nickel stub using carbon-loaded, double-sided adhesive tape (Agar Scientific, Stanstead, UK). AFM studies were carried out using the scanning probe microscope (Discoverer TopoMetrix® TMX2000 Scanning Probe Microscope, Veeco, Santa Barbara, CA, USA) in contact mode under atmospheric conditions (60–65% relative humidity, 295 K; HI 91610C microprocessor logging digital thermo-hygrometer, Hanna Instruments, London, UK), although for some experiments, a liquid cell was used. V-shaped, silicon nitride cantilevers (spring constant of 0.036 N m^{-1}) with integrated standard profile, square pyramidal tips (4 μm × 4 μm base, 4 μm height, 50 nm tip radius) were used. The sample was held in position on a piezo-electric tripod scanner capable of a maximum *x*, *y*, *z*-translation of 75 × 75 × 12 μm^3. Images were levelled (6th order) and selected images (500 lines × 500 pixels) were left-shaded to enhance topographical features.

2.11. Membrane electrode assembly (MEA) studies

Electrodes based on Toray TGP-H-060 carbon paper, gas diffusion media (GDM) screen printed with inks manufactured from Johnson Matthey Fuel Cell's HiSpec® 4000 (40%wtPt on Vulcan XC72R) electrocatalyst and aqueous Nafion® solution (1100 EW, 10%wt) were used at the cathode and anode. The electrodes were placed either side of the membrane and the package laminated at constant pressure and temperature to produce MEAs in bonded catalysed substrate (BCS) form.

The MEA performance was evaluated in a Ballard Mark 5E unit cell (240 cm^2 active geometrical area) fitted with internal membrane humidification. The MEAs were located between carbon flow field plates with silicone rubber seals located around the periphery of the plate to prevent external gas leakage. The unit cell was compressed to 800 kPa above the internal pressure of the cell using a bladder mechanism. A leak check was performed to ensure negligible external and internal leaks of gas or water.

The MEA was conditioned at a current density of 538 mA cm^{-2} under the selected test conditions (i.e. typically an inlet temperature of 80 °C, at p H_2/air of 400/400 kPa and a gas stoichiometry of H_2/air = 1.5/2.0) until the cell output potential had stabilised. After conditioning, the steady state cell output potential *versus* current density relationship of the MEA was recorded using H_2 and, in turn, air, helox (21% O_2 in helium) and O_2 were used as oxidants. At each current density the oxidant was switched on and given 30 min to stabilise the cell on air and 3 min each on helox and O_2. After the cell output potential was recorded on an O_2 stream the cell current was interrupted for 50 μs by a computer controlled switch and the resulting output potential step recorded using an oscilloscope. An average of four measurements was used to calculate the ohmic resistance.

The water balance in the MEA was examined at 538 mA cm^{-2}, 754 mA cm^{-2} and 1076 mA cm^{-2} by increasing the air stoichiometry from 2.0 to 10.0 while monitoring the change in the cell output potential.

3. Results and discussion

3.1. Water content, thickness and ion-exchange capacity

The ion-exchange capacities, equivalent weights, hydration numbers and thickness of the composite membranes containing different fillers are shown in Table 2. Selected values for extruded Nafion® membranes are included for comparison purposes. A wide variation in IX (0.83–1.37 mmol H^+ g^{-1}) and EW (729–1199 g polymer/SO_3H) was observed among the composite membranes. Most evident was that all of the higher loaded SiO_2 membranes (**3**, **6** and **8**) have higher IXs and lower EWs values than the unfilled cast Nafion® membrane **1**, the ZrO_2 membrane **9** and the TiO_2 membranes **10**–**13**. This suggests that the acidic SiO_2 oxide groups provide additional H^+ which consumes NaOH during the measurement of the IX or EW. In contrast, the ZrO_2 and TiO_2 oxides do not provide additional H^+. Apart from membrane 12 ('TiO_2-B'-5%wt), which may have a poor distribution of filler material, the remaining scatter in the IX or EW is typical of the variability in this measurement for Nafion® type membranes (see e.g. [3]). A closer comparison of membrane materials would necessitate allowances for the impact of the filler mass and characterisation of the filler distribution.

The water content of the filled membranes measured in pure water and H_2SO_4 (0.1 mol dm^{-3}) showed a larger variability than the extruded Nafion® series. All membranes apart from the 'TiO_2-B' membranes **12** and **13** showed a measurable decrease in the hydration state in H_2SO_4 compared to the values calculated for pure water. Generally at equilibrium, the water content is related not only to the hydration state of the charged species, mobile ions and fixed exchange groups present in the membrane phase, but also to the external electrolyte concentration which affects the value of the water activity in the membrane–solution system [27].

Table 2
Hydration properties and thickness of composite membranes (the Nafion NE materials are unfilled, extruded membranes).

Membrane type	Ion-exchange capacity [mmol $H^+ g^{-1}$]	Equivalent weight [g polymer per SO_3H]	Hydration number in H_2O [mol H_2O per mol SO_3H]	Hydration number in 1 mol dm^{-3} H_2SO_4 [mol H_2O per SO_3H]	Dry film thickness [μm]	Hydrated thickness (1 mol dm^{-3} H_2SO_4) [μm]	Percentage thickness increase on hydration
Nafion® NE-117	0.93	1071	23.2 ± 0.3	19.1 ± 0.7	186 ± 4	223 ± 8	20
Nafion® NE-115	0.99	1012	21.9 ± 0.7	18.8 ± 0.3	136 ± 2	157 ± 2	15
Nafion® NE-1135	0.98	1021	21.1 ± 0.7	18.3 ± 0.4	91 ± 2	110 ± 2	21
Nafion® NE-112	0.98	1026	20.7 ± 0.5	15.5 ± 0.2	51 ± 2	64 ± 2	26
1 (unfilled cast Nafion® membrane)	0.96	1044	31.6 ± 3.4	21.5 ± 0.8	34 ± 1	60 ± 8	77
2 (SiO_2-A, 5%wt)	0.95	1051	29.9 ± 1.9	22.7 ± 2.4	28 ± 1	60 ± 8	114
3 (SiO_2-A, 10%wt)	1.37	729	24.4 ± 0.8	16.3 ± 0.8	29 ± 2	56 ± 4	93
5 (SiO_2-B, 5%wt)	1.13	888	23.7 ± 1.7	18.7 ± 0.9	34 ± 3	57 ± 9	68
6 (SiO_2-B, 10%wt)	1.11	901	29.3 ± 2.3	21.2 ± 1.2	33 ± 2	55 ± 7	67
7 (SiO_2-C, 5%wt)	0.98	1003	33.7 ± 1.6	21.7 ± 0.5	34 ± 1	54 ± 5	59
8 (SiO_2-C, 10%wt)	1.03	968	40.9 ± 3.4	23.7 ± 0.7	33 ± 1	58 ± 5	76
9 (ZrO_2-A, 5%wt)	0.90	1106	30.4 ± 4.3	24.7 ± 3.0	30 ± 2	52 ± 9	63
10 (TiO_2-A, 5%wt)	0.92	1089	48.9 ± 1.4	36.8 ± 4.7	34 ± 3	62 ± 18	82
11 (TiO_2-A, 10%wt)	0.97	1030	59.9 ± 2.6	45.4 ± 3.0	33 ± 2	138 ± 18	318
12 (TiO_2-B, 5%wt)	0.83	1199	32.2 ± 2.0	32.8 ± 3.8	34 ± 3	118 ± 17	247
13 (TiO_2-B, 10%wt)	0.93	1075	53.7 ± 1.8	50.4 ± 3.2	32 ± 3	86 ± 13	169

For hydration in water, the water content values of the extruded Nafion® series were very close to a λ value of 22 mol H_2O per SO_3H, which is indicative of an immersed, fully hydrated membrane [28]. The corresponding λ values in H_2SO_4 were only slightly lower reflecting the high hydration level of the membranes. In water, however, the λ values for all the cast Nafion® composite membranes exceeded 22 mol H_2O per SO_3H. The λ of the unfilled cast Nafion® membrane **1** in water was 31.6 ± 3.4, reflecting the impact of the cast Nafion® ionomer and the quartz web on the ability of the composite membrane to intake up water. The casting process has been reported to give membranes with high water contents [17] and there is the possibility of open regions within the quartz web that could fill with water. Considering the SiO_2 membranes, the 'SiO_2-B' and 'SiO_2-C' structures both show an increase in the water take-up with higher SiO_2 filler level, suggesting the filler is impacting the water content. However, the 'SiO_2-A' sample did not show this trend which together with the low IX/high EW for membrane **2** ('SiO_2-A', 5%wt) might indicate a poor dispersion of the SiO_2 in this particular membrane sample. It is also clear that the SiO_2 fillers do not increase the λ values above the unfilled cast Nafion® membrane **1**. This is also true for membrane **9** ('ZrO_2', 5%wt). However, all of the TiO_2 membranes **10**–**13** are significantly more hydrated with λ values of 32.2–59.9 in water. The addition of more TiO_2 from 5%wt to 10%wt also significantly increases the water content from 48.9 to 59.9 in membranes **10** and **11** ('TiO_2-A') and from 32.2 to 53.7 for membranes **12** and **13** ('TiO_2-B'). This is probably due to the TiO_2 particles attracting water and becoming hydrated. The additional water content of the TiO_2 containing membranes might significantly reduce the need for external humidification if used as a membrane in PEM fuel cell applications.

The composite membranes had a much higher percentage increase in thickness upon hydration in H_2SO_4 (1 mol dm^{-3}) than the extruded Nafion® series of membranes. For example, the composite membrane **1** without filler showed a membrane thickness increase of approximately 77%, which is over three times higher than that seen for extruded Nafion® membranes [16] (e.g. Table 2). For the SiO_2-filled membranes (**2**, **3** and **5**–**8**) and the ZrO_2-filled membrane **9** the thickness increases were broadly comparable to membrane **1**. This suggests that the filler retained a similar state of hydration and the thickness increase must be related to expansion of the quartz web and its partial separation from the Nafion® polymer.

In contrast, membranes containing TiO_2 fillers showed extremely large increases in membrane thickness from 169% to 318% with only membrane **10** ('TiO_2-A', 5%wt) at 82% in-line with the other composite membranes, as shown in Table 2. This suggests that they may have formed a hydration sphere around the TiO_2 filler, causing significant areas of the membrane to become swollen.

3.2. DC resistance and conductivity measurements

The area resistance (*RA*) and thickness (*x*) of the composite membranes are shown in Fig. 2a and c with the corresponding plots of conductivity in Fig. 2b and d, respectively. Since the conductivity corrects the resistance for the variation in the membrane thickness it is a useful parameter for comparing the intrinsic conductivity of the membranes. However, the area resistance more closely reflects the performance of a given membrane as long as the hydrated thickness reflects the thickness of the membrane in practical operation. In the PEM fuel cell, this is dependent on MEA structure since in some structures the electrodes are bonded to the membrane, which constrains thickness increases; in other cell design architectures, this is not the case.

Fig. 2a shows that the unfilled cast Nafion® membrane **1** and the SiO_2-filled membranes **2**, **3** and **5**–**8** show reasonably close control

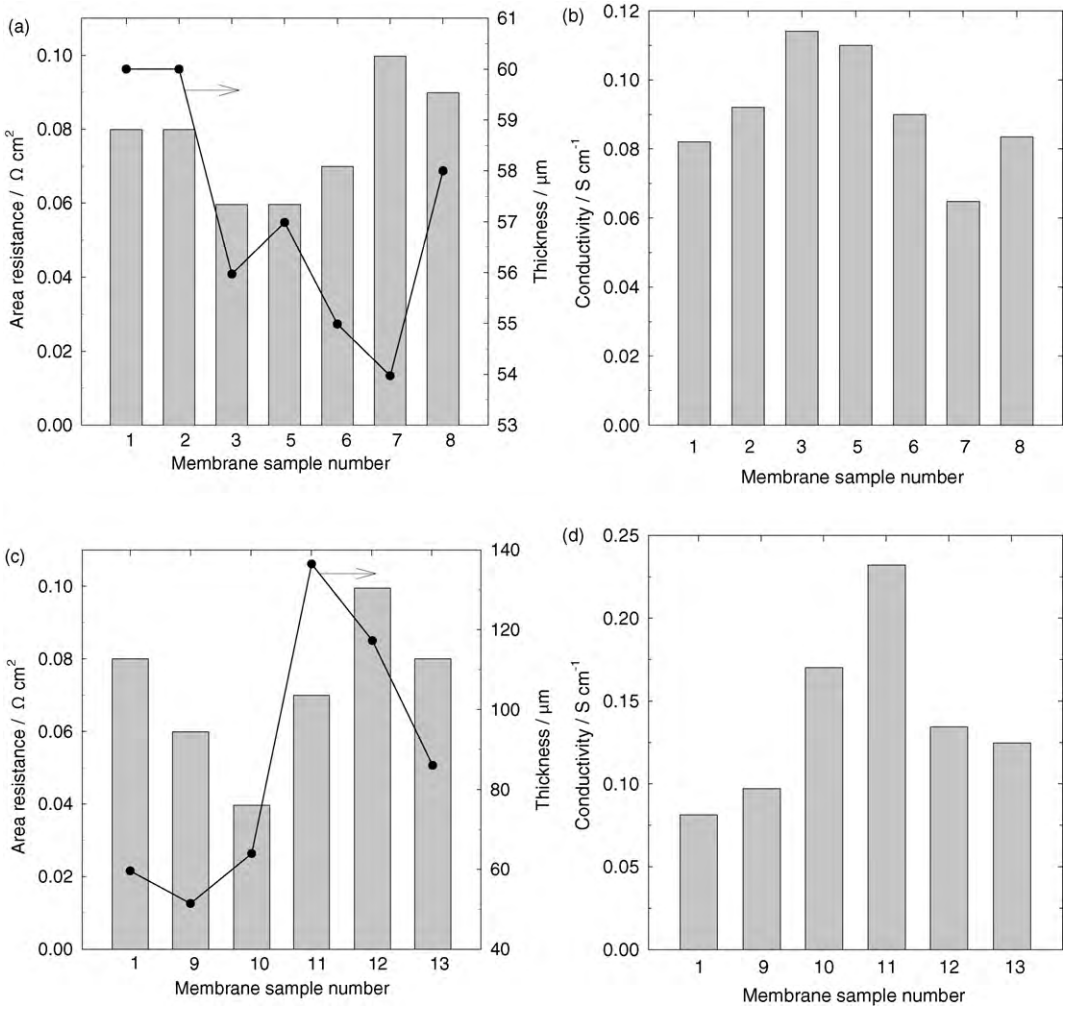

Fig. 2. Area resistance, membrane thickness (a, c) and proton conductivity (b, d) of composite membranes containing no filler (membrane **1**), SiO_2 fillers (membranes **2**, **3**, **5**–**8**), ZrO_2 filler (membrane **9**) and TiO_2 fillers (membranes **10**–**13**) in 1 mol dm^{-3} H_2SO_4 at 298 K. In a and c, the bars represent area resistance while the data points joint with a line are the thickness values.

of thickness at 54–60 μm in H_2SO_4 (0.1 mol dm^{-3}). The area resistances are also comparable in Fig. 2a as are the conductivities in Fig. 2b. This suggests the SiO_2 fillers have little impact on the conductivity of the membranes. This is also true of the ZrO_2 membrane **9** (Fig. 2c), which also showed a similar thickness and slightly lower area resistance to the unfilled cast Nafion® membrane **1** and the SiO_2-filled membranes **2**, **3** and **5**–**8** as shown in Fig. 2a.

The TiO_2-filled membranes showed a different behaviour. Both 'TiO_2-A'- and 'TiO_2-B'-filled membranes showed significantly higher conductivities than the unfilled composite Nafion® membrane. This is probably related to the high hydration number (Table 2). Fig. 2d shows that 'TiO_2-A'-filled membranes **10** and **11** produced conductivities of 0.17 S cm^{-1} at 5%wt fill and 0.23 S cm^{-1} at 10%wt fill, respectively. Interestingly, the higher fill level did produce further benefit in terms of conductivity. Even although the membranes are thicker, the high conductivity gave rise to lower area resistance in Fig. 2c compared to the unfilled cast Nafion® membrane **1**.

'TiO_2-B'-filled membranes did not show such high conductivities and the addition level of TiO_2 has little impact on the conductivity (Fig. 2d). This may reflect an interaction between the TiO_2 and the Nafion® ionomer reducing the H^+ mobility in the 'TiO_2-B'-filled membranes (see Section 2.2). Consequently, membrane **12** ('TiO_2-B', 5%wt) showed a higher area resistance compared to the unfilled cast Nafion® membrane **1**, since it is thicker, and membrane **13** ('TiO_2-B', 10%wt) shows a similar area resistance since it had a similar thickness (Fig. 2c).

3.3. Four-point probe measurements

Four-point probe measurements were performed on extruded Nafion® NE-112 membrane (for comparison), on the quartz web with organic Nafion® binder and on the composite membranes without filler and with ZrO_2 and TiO_2 fillers. The highest electrical resistivity was obtained from the quartz web with Nafion® binder (30.1 ± 0.3 kΩ cm), demonstrating the higher electrical conductivity of the Nafion® ionomer both without and with metal oxide filler. For example, the unfilled cast Nafion® membrane **1** was much less resistive at 14.1 ± 5.1 kΩ cm, which was similar to the electrical resistivity of 12.9 ± 2.2 kΩ cm for extruded Nafion® NE-112. It appears that, in the presence of a Nafion® ionomer fill, the electrical resistivity of the quartz web has little impact and the Nafion® dominates the electrical resistivity of the membrane.

Considering the impact of the filler metal oxides membrane **9** (ZrO_2, 5%wt) had a slightly increased electrical resistivity of 17.1 ± 5.0 kΩ cm compared to the unfilled cast Nafion® membrane **1**. The TiO_2 membranes **10** ('TiO_2-A', 5%wt) and **11** ('TiO_2-A', 10%wt) had similar electrical resistivities to the unfilled cast Nafion® membrane **1** of 10.8 ± 3.2 kΩ cm and 13.0 ± 3.3 kΩ cm, respectively. However, the 'TiO_2-B' membranes **12** ('TiO_2-B', 5%wt) and **13** ('TiO_2-

B', 10%wt) had lower electrical resistivities of $8.3 \pm 2.9\,k\Omega\,cm$ and $8.6 \pm 2.4\,k\Omega\,cm$, respectively. This suggests that the 'TiO_2-B' to Nafion® interactions result in a lower proton conductivity by reducing proton mobility by altering the distribution of TiO_2 in the ionomer.

3.4. Scanning electron microscopy

SEM imaging of the quartz web showed that the fibre distribution was random, with fibre lengths extending from 50 to several hundred microns, as seen in Fig. 3a; with fibre diameters typically between 1 μm and 7 μm. The quartz web samples treated with the organic Nafion® binder showed regions where thin films of ionomer bridged across some of the fibres (Fig. 3b). This bridging allowed subsequent impregnation and then coating of the quartz web without dissolution into the ionomer solution.

Under SEM observation, the final membranes showed a coating of ionomer that completely covered both sides of the quartz web structure. The quartz web thickness was typically 10 μm, which is approximately 30% of the total membrane sheet thickness, with coatings of Nafion® ionomer of around 10 μm thickness on each face to give a final membrane sheet thickness of approximately 30 μm. In some isolated regions of the quartz web with initial Nafion® impregnation and coating (before final spraying) there were longitudinal defects which suggested some removal of individual quartz fibres. This does raise some concern about the mechanical strength of the Nafion® ionomer to quartz bond. This also supported the need to perform a final spray coating of both faces of the membrane to ensure any gaps in the ionomer coating of the quartz web due to the deficiencies in the laboratory method of manufacture were covered. Such gaps during manual production of membrane sheet were unavoidable (see e.g. Fig. 3c). In volume production, web manufacture and Nafion® ionomer coating are expected to be much more defect-free.

3.5. Atomic force microscopy

The surface of extruded Nafion® NE-117 appeared very flat (R_a = 5 nm, Table 3), with a few raised features, as seen in Fig. 4a, which may be due to contamination. The percentage surface area difference ($\%\Delta A_s$) between real (A_r) and projected surface area ($A_p = 100\,\mu m^2$) as given by:

$$\%\Delta A_s = 100\left(\frac{A_r - A_p}{A_r}\right) \quad (4)$$

was 0.5%, confirming the high surface flatness of this membrane.

AFM imaging of the quartz web with or without organic Nafion® binder was not possible due to the roughness of the surfaces combined with the limited *z*-range of the piezo-electric scanner. The unfilled cast Nafion® membrane **1**, imaged under atmospheric conditions, exhibited a much rougher surface (R_a = 74 nm, $\%\Delta A_s$ = 19.2%) than the extruded Nafion® NE-117 (R_a = 5 nm, $\%\Delta A_s$ = 0.5%), as shown by the comparison between Fig. 4b and a. The high surface roughness reflects the impact of the quartz web structure in minimising the dimensional change of the ionomer in the *x*–*y* plane of the membrane, as it changes hydration level.

Table 3 shows that, under atmospheric conditions, all of the composite membranes had an average surface roughness (R_A) (19–47 nm) and surface area difference (2.6–12%) intermediate between the very flat extruded Nafion® NE-117 and the rougher unfilled cast Nafion® membrane **1**. This intermediate character is shown for membrane **2** ('SiO_2-A', 5%wt) and membrane **10** ('TiO_2-A', 5%wt) in Fig. 4c and d respectively by comparison with Fig. 4a for extruded Nafion® NE-117 and Fig. 4b for unfilled cast Nafion® membrane **1**. This probably reflects the impact of the filler in reducing the dimensional change of the composite membrane. Table 3

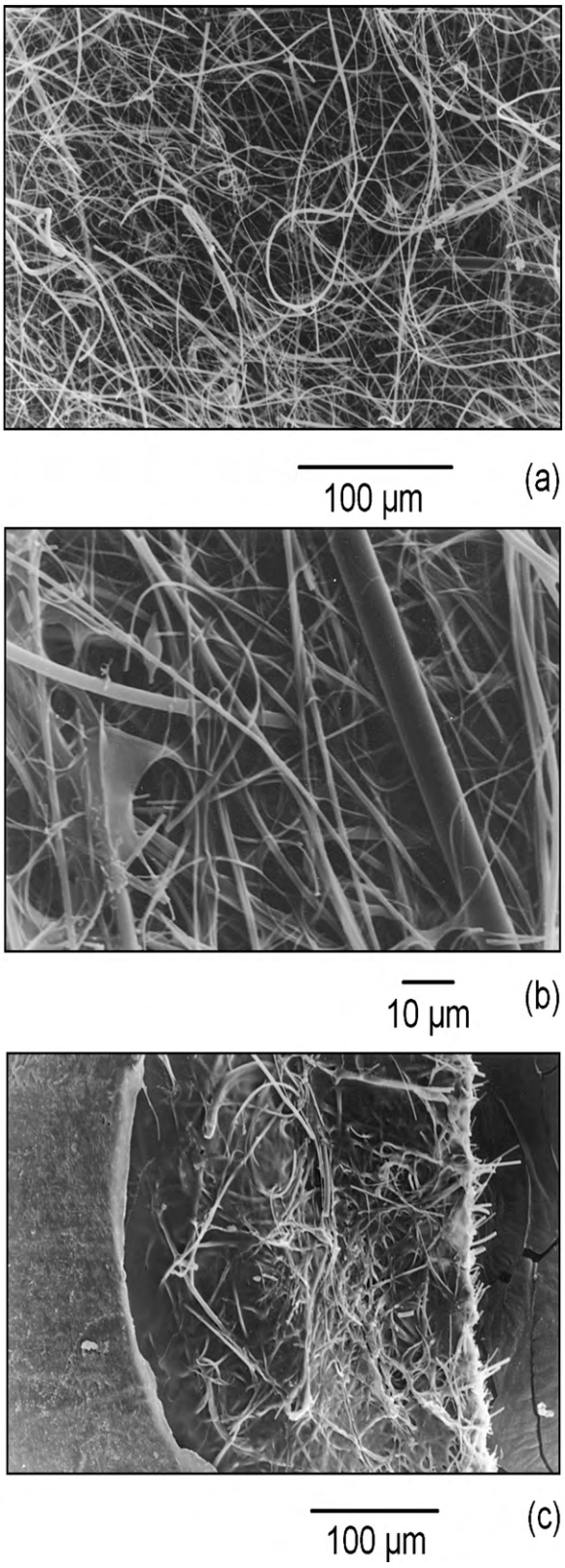

Fig. 3. SEM images of (a) quartz web structure, (b) quartz web with Nafion® as a binder and (c) composite membrane **5** ('SiO_2-B', 5%wt) before final spray coating.

Table 3
AFM surface roughness and area measurements (area: 10 μm × 10 μm).

Membrane type	Arithmetic roughness average, R_A (nm) [29]	Root mean square roughness, RMS (nm) [29]	Average peak-to-valley roughness, R_z (nm)	% Difference in surface area
Atmospheric conditions				
Nafion® NE-117 (unfilled, extruded, membrane)	5	6	111	0.5
1 (unfilled cast Nafion® membrane)	74	95	362	19.2
2 (SiO_2-A, 5%wt)	41	5	174	6.3
3 (SiO_2-A, 10%wt)	25	33	126	2.6
5 (SiO_2-B, 5%wt)	38	50	288	12.0
6 (SiO_2-B, 10%wt)	33	44	140	4.3
7 (SiO_2-C, 5%wt)	19	93	239	2.6
9 (ZrO_2-A, 5%wt)	39	50	228	10.0
10 (TiO_2-A, 5%wt)	47	59	204	9.5
11 (TiO_2-A, 10%wt)	24	32	153	10.8
Fully hydrated				
Nafion® NE-117 (unfilled, extruded, membrane)	8	13	104	4.0
1 (unfilled cast Nafion® membrane)	38	51	234	6.5
5 (SiO_2-B, 5%wt)	26	33	148	4.2

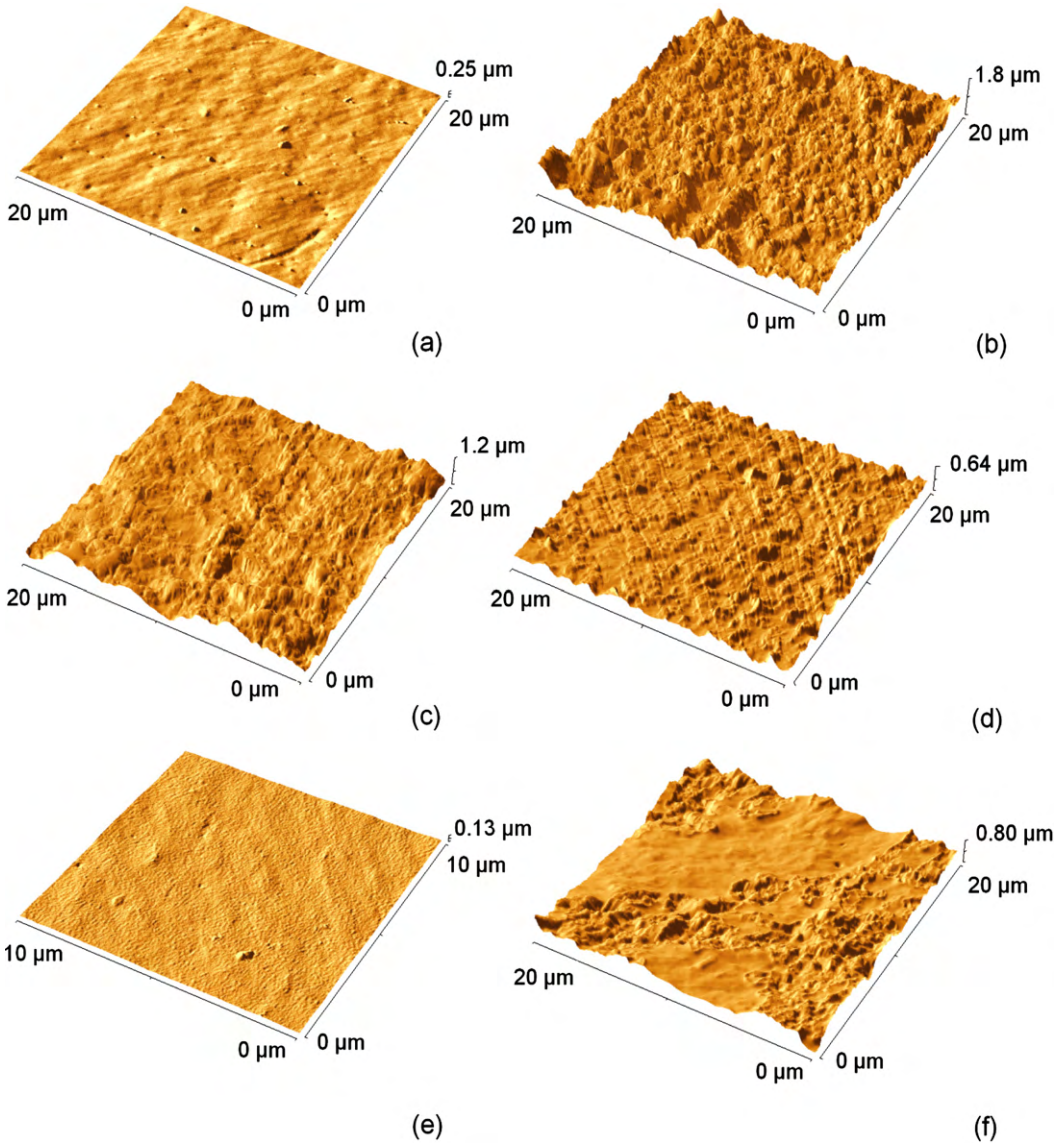

Fig. 4. AFM images of (a) extruded Nafion® NE-117 membrane, (b) composite membrane **1** (unfilled cast Nafion®), (c) composite membrane **2** ('SiO_2-A', 5%wt) and (d) composite membrane **10** ('TiO_2-A', 5%wt) all under atmospheric conditions; and (e) extruded Nafion® NE-117 membrane and (f) composite membrane **1** (unfilled cast Nafion®) both under fully hydrated conditions.

also shows that for 'SiO_2-A', 'SiO_2-B' and 'TiO_2-A' composite membranes an increase in the additive content from 5%wt to 10%wt resulted in a decrease in surface roughness reflecting the greater restriction of the dimensional change of the membrane.

Fig. 4c and d also show the appearance of ridges for membrane **2** ('SiO_2-A', 5%wt) and membrane **10** ('TiO_2-A', 5%wt). This may be due to the rolling of the cast membrane during manufacture. The ridges were not always present in the composite membranes.

To investigate the effect of hydration on membrane topography, extruded Nafion® NE-117, unfilled cast Nafion® membrane **1** and composite membrane **5** ('SiO_2-B', 5%wt) were examined in water. Extruded Nafion® NE-117 had a slightly higher surface roughness (8 from 5 nm) and % difference in surface area (4 from 0.5%) in water compared to atmospheric conditions. Comparison of Fig. 4e with Fig. 4a shows the negligible visual change in the surface roughness between hydrated and atmospheric conditions. The small difference is probably due to swelling of the membrane on hydration.

In contrast, the surface roughness (38 from 74 nm) and % difference in surface area (6.5 from 19.2%) is significantly lower for the wet, hydrated unfilled cast Nafion® membrane **1**. This is shown visually by comparing Fig. 4b (atmospheric) with Fig. 4f (wet, hydrated). The images show that hydration does significantly reduce the surface membrane roughness over much of the surface area but that there are regions that still exhibit a reasonable degree of surface roughness. This suggests that the Nafion® ionomer fill swells on hydration and the quartz web does not prevent significant *x*–*y* dimensional change in these regions, allowing the membrane to flatten. In other regions, the quartz web prevents *x*–*y* dimensional change and the surface roughness is retained. Table 3 also shows that composite membrane **5** ('SiO_2-B', 5%wt) shows a similar behaviour on hydration. The surface roughness (26 from 38 nm) and the % difference in surface area (4.2 from 12.0%) are both significantly reduced in water compared to atmospheric conditions.

3.6. MEA results

Based on the negligible impact on *ex-situ* proton conductivity from the addition of significant quantities of SiO_2 to the Nafion® cast composite membrane sheets the performance in a Ballard Mark 5E unit cell was investigated.

To provide a more robust composite membrane, two sheets were laminated together to produce a final membrane with a target thickness of 60 μm for PEM fuel cell testing. Membranes were produced which had 5%wt and 20%wt 'SiO_2-A' and 5%wt 'SiO_2-C'. Fig. 5 shows the cell output potential *versus* current density performance of the cast membrane samples with H_2 as fuel and air, helox or pure O_2 as oxidant. This shows that at very low current densities the SiO_2 fillers in the membrane have little impact on the performance of the MEAs relative to the MEA based on the cast membrane without filler. In this current density region the performance is controlled by the sluggish rate of O_2 reduction at the cathode and by the utilisation of the Pt catalyst in the cathode catalyst layer. This suggests the membrane filler is not impacting the bulk proton conduction in the cathode catalyst layer to such an extent that it impacts performance at such low current densities, which would lower the catalyst utilisation. At higher current densities, however, the performance from the SiO_2-filled membranes is lower.

Fig. 5 also shows that compared to the performance on pure O_2 the performance with air as oxidant is more separated at high current densities. The clear order of performance is cast membrane without filler > 5%wt Ludox® > 20%wt Ludox® > 5%wt Aerosil®. With air as oxidant mass transport in the cathode catalyst layer and the GDM can in adverse cases impact the MEA performance. This can be investigated at each current density by

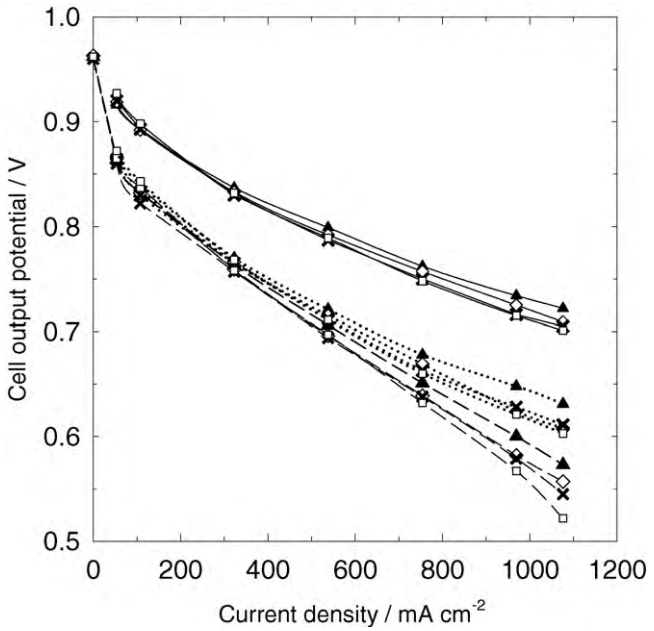

Fig. 5. Unit cell performance of the composite membranes based MEAs in a Ballard Mark 5E unit cell operating with full internal humidification at 80 °C. H_2/air (dashed lines), helox (dotted lines) or pure O_2 (solid lines) at 400/400 kPa and 1.5/2.0, 2.0, 10.0 inlet gas stoichiometries. Air, no filler in membrane (▲), air, 5%wt Ludox in membrane (◊), air, 20%wt Ludox in membrane (×), air, 5%wt Aerosil in membrane (□).

subtracting the performance on helox from the pure O_2 performance to give the O_2 gains and the performance on air from the helox performance to give the helox gains. As a first approximation the O_2 gains give an indication of the O_2 permeability losses and the helox gains the O_2 gas diffusion losses in the cathode.

Considering the performance with pure O_2 as an oxidant, the higher current density performance is normally controlled by the proton conductivity of the membrane. It is possible to fit the pure O_2 data by a non-linear least squares analysis of Eq. (5) [30], using the Levenberg–Marquardt procedure [31], to obtain an average value for the MEA resistance over the pseudo-linear region of the cell output potential *versus* current density plot.

$$E_{cell} = (E_{cell,r} + b_c \log A_{j_o}) - b_c \log A_j - AjR \quad (5)$$

where E_{cell} is the cell potential, $E_{cell,r}$ is the reversible cell potential, j_o is the exchange current density, b_c is the cathodic Tafel slope for oxygen reduction and R represents the ohmic resistance of the MEA and any mass transport losses at the cathode (the latter normally being negligible with pure O_2).

The cast membrane without filler had an MEA resistance of 0.11 Ω cm^2, whereas the 'SiO_2-A' MEAs had values of 0.12 Ω cm^2 and the 'SiO_2-C' MEA showed the highest resistance of 0.13 Ω cm^2. The current-interrupt method was also used to look at the bulk membrane conductivity. Fig. 6 shows that the current-interrupt resistance was similar for the filled membranes and for the cast membrane without filler. This is in agreement with the *ex-situ* proton conductivity measurements on the membranes shown in Fig. 2b.

This difference in the curve-fitted MEA resistance and the bulk membrane resistance suggests either an increase in the cathode catalyst layer resistance or a small increase in the interfacial resistance between the cast membranes with filler and the cathode catalyst layer introducing a small proton conduction barrier. Both effects may be due to modification of the water flux within the MEA. Interestingly increasing the 'SiO_2-A' loading from 5%wt and 20%wt did not increase the resistance further. The higher MEA resistance

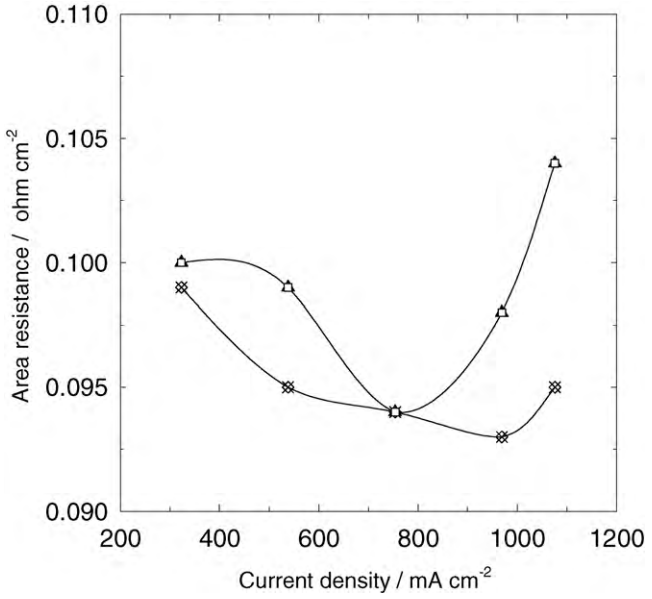

Fig. 6. Current-interrupt resistance *versus* current density of the composite membrane based MEAs. Ballard Mark 5E unit cell operating with full internal humidification at 80 °C with H_2/air, helox or pure O_2 at 400/400 kPa and 1.5/2.0, 2.0, 10.0 inlet gas stoichiometries. Air, no filler in membrane (▲), air, 5%wt Ludox in membrane (◊), air, 20%wt Ludox in membrane (×), air, 5%wt Aerosil in membrane (□).

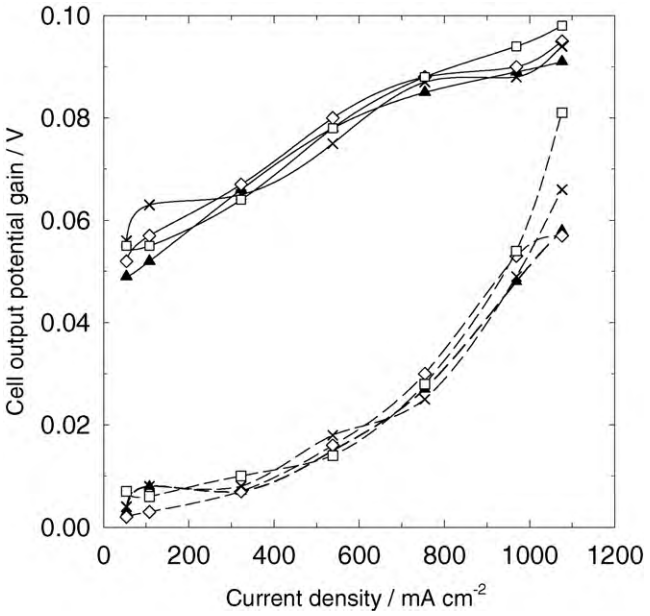

Fig. 8. Helox (dashed lines) and oxygen cell value gains (solid lines) *versus* current density for the composite membrane based MEAs. Ballard Mark 5E unit cell operating with full internal humidification at 80 °C with H_2/air, helox or pure O_2 at 400/400 kPa and 1.5/2.0, 2.0, 10.0 inlet gas stoichiometries. Helox gains, no filler in membrane (▲), helox gains, 5%wt Ludox in membrane (◊), helox gains, 20%wt Ludox in membrane (×), helox gains, 5%wt Aerosil in membrane (□).

with the 'SiO_2-C' at a loading of 5%wt confirms a larger impact perhaps due to a poorer distribution of the SiO_2 using the Aerosil® powder compared with the Ludox® dispersion.

Fig. 7 compares the specific resistance of the cast membrane based MEAs with the corresponding MEAs based on the extruded Nafion® series of membranes. The resistances were measured using the current-interrupt technique and reflect the bulk membrane resistance. This shows that the cast membranes are broadly inline with the response of the extruded Nafion® membranes. The increase in the specific resistance of the extruded Nafion® membranes as thickness decreases has been ascribed to a surface effect produced during the extrusion process increasing the resistance [16]. The membrane surface makes a larger contribution to the total resistance as thickness decreases. Further studies are required to confirm the reason for the similar response of the cast membranes either without or with filler, although, the filler does not appear to be a major factor and studies have shown surface effects can also be produced from cast membranes [17].

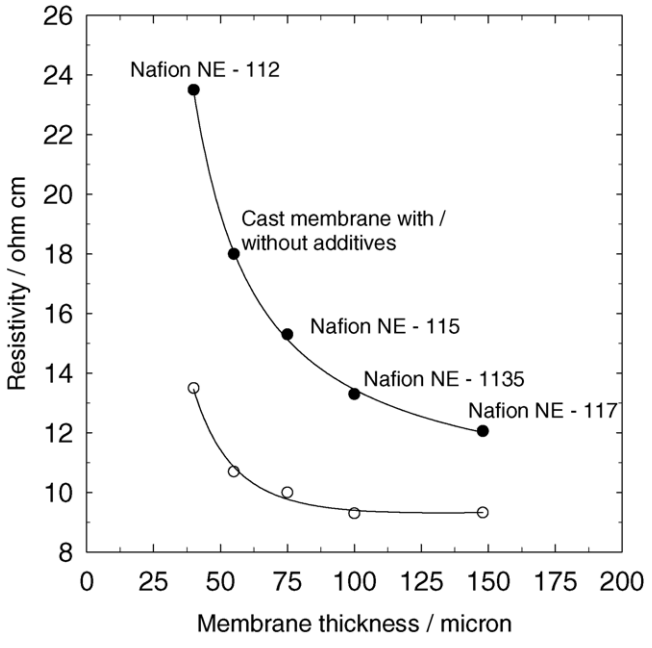

Fig. 7. Resistivity *versus* membrane thickness of the Nafion® series of extruded membranes and the cast composite membranes. The hardware and Toray carbon paper substrate resistance was measured as 0.04 Ω cm^2 using a two point dc probe, which was subtracted from the total measured MEA resistance to give the hardware corrected data. Ballard Mark 5E unit cell operating with full internal humidification at 80 °C with H_2/air, helox or pure O_2 at 400/400 kPa and 1.5/2.0, 2.0, 10.0 inlet gas stoichiometries. Raw data (●), data hardware corrected for IR drop (○).

Fig. 8 shows that the O_2 gains are comparable for all of the cast membrane based MEAs. The gain of *ca.* 59 mV at low current density is due to the increase in the O_2 partial pressure moving from helox to pure O_2. The higher gains at higher current densities are due to increased O_2 permeability losses as the rate of O_2 reduction and the rate of water production in the cathode increases. Fig. 8 shows that the helox gains are similar for all of the composite membrane based MEAs, with the increasing helox gains at higher current density ascribed again to the increased rate of O_2 reduction and water production. In conclusion, the SiO_2 fillers have not significantly impacted either the O_2 permeability or the rate of O_2 diffusion in the cathode of the MEAs at the higher current densities.

Based on the results of the O_2 and the helox gain tests, an initial examination of the water balance in the cathode was performed to establish if this was the route cause of the more variable performance on air. Table 4 shows the change in the cell output potential for each of the MEAs at 538 mA cm^{-2}, 754 mA cm^{-2} and 1076 mA cm^{-2} as the air stoichiometry was increased by a factor of 5 (from 2.0 to 10.0). Such an air purge removes water initially from the cathode catalyst layer and GDM then from the membrane.

For the cast membrane without filler, the cell output potential increased by 21 mV at 538 mA cm^{-2}, 29 mV at 754 mA cm^{-2} and 53 mV at 1076 mA cm^{-2}. This is typical for a Nafion® membrane based MEA in the Ballard Mark 5E unit cell operating at 80 °C and 400 kPa with full internal humidification. The increase

Table 4
Air purge response of the MEAs in a Ballard Mark unit 5E cell.

Current density ($mA\,cm^{-2}$)	Membrane type	Change in cell output potential (V)
538	Unfilled cast	0.021
	5%wt 'SiO_2-A' (Ludox)	0.016
	20%wt 'SiO_2-A' (Ludox)	0.007
	5%wt 'SiO_2-C' (Aerosil)	−0.001
754	Unfilled cast	0.029
	5%wt 'SiO_2-A' (Ludox)	0.019
	20%wt 'SiO_2-A' (Ludox)	0.007
	5%wt 'SiO_2-C' (Aerosil)	0.002
1076	Unfilled cast	0.053
	5%wt 'SiO_2-A' (Ludox)	0.047
	20%wt 'SiO_2-A' (Ludox)	0.025
	5%wt 'SiO_2-C' (Aerosil)	0.013

in cell output potential reflects the impact of moving water from the cathode catalyst layer and GDM. The MEA typically runs slightly wet to ensure good membrane humidification, while accepting the increase in the mass transport losses at the cathode which increase at higher current densities due to the increased rate of water production, as shown by the helox and O_2 gains (e.g. Fig. 8). The 5%wt SiO_2-A membrane based MEA shows the closest response to the unfilled cast Nafion® membrane without filler with corresponding increases in cell output potential of 16 mV at 538 $mA\,cm^{-2}$, 19 mV at 754 $mA\,cm^{-2}$ and 47 mV at 1076 $mA\,cm^{-2}$. The 20%wt SiO_2-A membrane based MEA is, however, running much drier as shown by the much lower cell output potential gains of 7 mV at 538 $mA\,cm^{-2}$, 7 mV at 754 $mA\,cm^{-2}$ and 25 mV at 1076 $mA\,cm^{-2}$ and the 5%wt SiO_2-C membrane is much drier with a cell output potential loss of −1 mV at 538 $mA\,cm^{-2}$ (due to membrane drying) and small gains of 2 mV at 754 $mA\,cm^{-2}$ and 13 mV at 1076 $mA\,cm^{-2}$. This suggests that the cause of the additional performance drop with the SiO_2-filled membranes (especially the 20%wt 'SiO_2-A' and 5%wt 'SiO_2-C' membranes) is drying of the cathode catalyst layer leading to lower proton conductivity. This drying may also have impacted on the interface between the cathode catalyst layer and the membrane. This suggests the SiO_2 fillers have changed the water flux in the MEA at the higher current densities through modification of the electroosmotic drag or the rate of water back-diffusion. More detailed studies are required to resolve this effect.

4. Conclusions

1. The ZrO_2- and TiO_2-filled composite membranes did not provide additional protons to significantly affect the IX or EW. In contrast, the EW values for the SiO_2 membranes were lowered by a contribution from the acidic metal oxide.
2. The cast composite Nafion® membranes all showed a greater water take-up and thickness increase than the extruded Nafion® membranes. The SiO_2 and ZrO_2 fillers did not significantly impact these properties but the TiO_2 filler significantly increased both water take-up and thickness increase. This may be beneficial for reducing the external humidification requirements of the PEM fuel cell stack.
3. The SiO_2 and ZrO_2 fillers had little impact on the cast Nafion® membrane proton conductivity. The 'TiO_2-A'- and 'TiO_2-B'-filled composite membranes both showed higher proton conductivity, especially the 'TiO_2-A'-filled membranes. This is probably due to the high water take-up, with 'TiO_2-B' to Nafion® ionomer interactions lowering the proton conductivity a little compared to the 'TiO_2-A'-filled membranes.
4. The electrical conductivity of the composite membranes is dominated by the Nafion® ionomer fill. The 'ZrO_2' and 'TiO_2-A' fillers have little impact, although, the 'TiO_2-B' filler increases electrical conductivity. This could be due to the impact of the 'TiO_2-B' to Nafion® ionomer interactions.
5. Final spraying of both faces of the Nafion® ionomer based quartz web structure was important to cover defects. The composite membranes had a central quartz web (*ca.* 10 μm thick) with 10 μm thick ionomer layers either side of the web. There were indications that fibre loss from the quartz web might be problematical.
6. The cast Nafion® composite membranes showed much higher surface roughness and a larger difference in surface area than the very flat extruded Nafion® NE-117. This was attributed to a restriction in the *x*–*y* dimensions by the quartz web as the ionomer swells. The SiO_2, ZrO_2 and TiO_2 fillers lowered the swelling and reduced the surface roughness and % difference in surface area. Full hydration of the composite membranes also lowered the surface roughness and percentage difference in surface area by allowing *x*–*y* dimensional change in some regions of the membrane.
7. The addition of SiO_2 fillers did lower the MEA performance at high current densities, with 'SiO_2-C' having the largest effect. Moving from 5%wt to 20%wt 'SiO_2-A' had only a small additional effect and there might be scope to increase 'SiO_2-A' loadings further to improve MEA cost effectiveness.
8. The lower performance of the SiO_2-filled membranes is not due to an increase in the bulk membrane resistance but to a reduction in the rate of the water flux to the cathode decreasing the proton conductivity within the cathode catalyst layer and perhaps also at the interface with the membrane.

Further work is necessary to correlate the physical and structural properties of the filler material (e.g. particle shape and size distribution) and the quality of the filler dispersion within the materials on the proton conduction of composite membranes.

Acknowledgements

The authors are grateful to the EPSRC for a CASE award to Sharon Slade *via* Johnson Matthey Technology Centre, Reading, UK. Torquil Landen and Darshini Fongalland (JMTC) kindly provided some materials and assisted with materials characterisation.

References

[1] K.A. Mauritz, R.B. Moore, Chem. Rev. 104 (2004) 4535.
[2] F. Delime, J.M. Leger, C. Lamy, J. Appl. Electrochem. 28 (1998) 27.
[3] D.E. Curtin, R.D. Lousenberg, T.J. Henry, P.C. Tangeman, M.E. Tisack, J. Power Sources 131 (2004) 41.
[4] V.P. McConnell, Fuel Cells Bull. 12 (2009) 12.
[5] F.C. Walsh, A First Course in Electrochemical Engineering, The Electrochemical Consultancy, Romsey, 1991.
[6] T.A. Davies, J.D. Genders, D. Pletcher, Ion Permeable Membranes, The Electrochemical Consultancy, Romsey, 1997.
[7] S.-A. Sheppard, S.A. Campbell, J.R. Smith, G.W. Lloyd, T.R. Ralph, F.C. Walsh, Analyst 123 (1998) 1923.
[8] T. Sata, Ion Exchange Membranes: Preparation, Characterization, Modification and Application, Royal Society of Chemistry, 2004.
[9] H. Strathmann, Ion-Exchange Membrane Separation Processes, Elsevier, 2004.
[10] A.B. Koltuniewicz, E. Drioli, Membranes in Clean Technologies: Theory and Practice, Wiley-VCH, Weinhem, FDR, 2008.
[11] T.R. Ralph, Platinum Met. Rev. 41 (1997) 102.
[12] G. Pourcelly, C. Gavach, in: P. Colomban (Ed.), Chemistry of Solid State Materials 2; Proton Conductors, Solids, Membranes and Gels, Materials and Devices, Cambridge University Press, 1992.
[13] J. Halim, F.N. Buchi, O. Haas, M. Stamm, G.G. Scherer, Electrochim. Acta 39 (1994) 1303.
[14] H.L. Yeager, A. Steck, J. Electrochem Soc. 128 (1981) 1880.
[15] T.D. Gierke, W.Y. Hsu, in: H.L. Yeager, A. Eisenberg (Eds.), Perfluorinated Ionomer Membranes, ACS Symposium Series No. 180, American Chemical Society, Washington, DC, 1982, p. 283.
[16] S. Slade, S.A. Campbell, T.R. Ralph, F.C. Walsh, J. Electrochem. Soc. 149 (2002) A1556.
[17] S. Slade, T.R. Ralph, C. Ponce de León, S.A. Campbell, F.C. Walsh, Fuel Cells (2009), doi:10.1002/fuce.200900118.

[18] R.A. Zoppi, S.P. Nunes, J. Electroanal. Chem. 445 (1998) 39.
[19] K.A. Mauritz, Mater. Sci. Eng. C6 (1998) 121.
[20] S.K. Tiwari, S.K. Nema, Y.K. Agarwal, Thermochim. Acta 317 (1998) 175.
[21] P. Costamaga, C. Yang, A.B. Bocarsly, S. Srinivasan, Electrochim. Acta 47 (2002) 1023.
[22] C. Yang, P. Costamaga, S. Srinivasan, J. Benziger, A.B. Bocarsly, J. Power Sources 103 (2001) 1.
[23] M. Watanabe, H. Uchida, Y. Seki, M. Emori, P. Stonehart, J. Electrochem. Soc. 143 (1996) 3847.
[24] J.A. Kolde, B. Bahar, M.S. Wilson, T.A. Zawodzinski, S. Gottesfeld, in: S. Gottesfeld, G. Halpert, A. Landgrebe (Eds.), Proton Conducting Membrane Fuel Cells I, Proceedings, vol. 95-23, The Electrochemical Society, Pennington, 1995, p. 193.
[25] T. Arimura, D. Ostrovskii, T. Okada, G. Xie, Solid State Ionics 118 (1999) 1.
[26] C.L. Gardner, A.V. Anantarama, J. Electroanal. Chem. 449 (1998) 209.
[27] G. Pourcelly, C. Gavach, in: P. Colomban (Ed.), Chemistry of Solid State Materials 2; Proton Conductors, Solids, Membranes and Gels, Materials and Devices, Cambridge University Press, 1992.
[28] T.A. Zawodzinski, M. Neeman, L.O. Sillerud, S. Gottesfeld, J. Phys. Chem. 95 (1991) 6040.
[29] J.R. Smith, S. Breakspear, S.A. Campbell, Trans. Inst. Met. Finish. 81 (2003) B55.
[30] R. Mosdale, S. Srinivasan, Electrochim. Acta 40 (1995) 413.
[31] W.H. Press, B.P. Flannery, S.A. Teukolsky, W.T. Vetterling, Numerical Recipes: The Art of Scientific Computing, Cambridge University Press, Cambridge, 1986, p. 523.